한국소성가공학회 2009년도 추계학술대회 논문집 pp. 33~37

프랙탈 표면을 가진 공구와 재료의 마이크로 접촉거동해석

김영석(경북대), 현상일(한국세라믹스기술원)

Microcontacting behaviour of material with fractal rough surface

Young-Suk Kim[1], Sang-Il Hyun[2]

Abstract

Finite-element methods are used to study non-adhesive, frictionless rough contact of elastic and plastic solids. Roughness on spherical surfaces is realized by self-affine fractal. True contact area between the rough surfaces and flat rigid surfaces increases with power law under external normal loads. The power exponent is sensitive to surface roughness as well as the curvature of spherical geometry. Surface contact pressures are analyzed and compared for the elastic and plastic solids. Distributions of local contact pressure are shown dependent on the surface roughness and the yield stress of plastic solids.

Keywords: Finite element method, Nano-contacts, Self-affine fractal surface.

1. Introduction

Contact analysis between two surfaces have been studied for the characterization of mechanical, electrical, and fluidic devices in the wide range of length scales [1]. As the size of devices can reach down to nanometer length scale recently, the contact analysis becomes more important in small length scale because of the dominated surface effect over bulk effect. Numerous analytical and numerical studies have been performed to examine how contact properties of surfaces are connected to surface geometries in contact [2-7]. It is well known real surfaces have always roughness in small length scale, which can be ignored in macroscopic scale. Besides the surface roughness at the contact, nominal shapes of contact surfaces were also investigated, which include flat, spherical, and pyramidal shapes.

In this paper, we considered spherical contact surfaces with roughness to examine how the contact properties are connected to the geometrical parameters such as curvature and roughness. True contact area vs. external load and contact pressure distributions were mainly considered as contact characteristics. To address on the dependence on materials properties, we used both elastic and plastic materials in the analysis.

2. Theoretical Background

2.1 Self-affine Fractal Surface and Roughness

Experimental measurements [8-10] on surface profile show the surface can be realized by self-affine fractal surface [11] in small length scale. Vertical height profiles (h) of self-affine surfaces show power scaling behavior as a function of the horizontal length scale (l), where the power exponent α is given by

$$h \propto l^{\alpha} . \qquad (1)$$

From the self-affine surface with height profile $h(x,y)$ at a point on x-y plane, the roughness Δ at small length scale is represented by

$$\Delta \equiv \sqrt{\langle |\nabla h|^2 \rangle / 2} \qquad (2)$$

where $\langle ... \rangle$ is the spatial average over x-y plane [7]. In the case of nominally flat surfaces, true contact

area under external normal load is shown mainly dependent on the local roughness Δ.

2.2 True Contact Area for Rough Surfaces

Interfacial characteristics between two surfaces can be determined by true contact area. In small length scale, however, the true contact area is significantly smaller than the nominal contact area [2]. True contact area as a function of external load has been investigated in numerous studies. True contact area (ϕ) is defined by the ratio between true contact area (A) over nominal contact area (A_0). It is well know the true contact area is represented as a power function of external load (P) by

$$\phi \propto \left(\frac{P}{E'}\right)^{\varepsilon} \quad . \qquad (3)$$

In the equation, E' is effective Young's modulus defined by $E' = E/(1-\nu^2)$ when E is Young's modulus and ν is Poisson's ratio and is the power exponent. At small loads, the power exponent is given by 2/3 for Hertzian spherical contact with no roughness, and 1 (linear) for nominally flat surface with roughness. The linear curve implies the true contact area increases as the external load to keep the average contact pressure remains constant.

3. Finite Element model and simulation

3.1 Modelling of Rough Surfaces

Successive random point algorithm [12] was introduced to generate self-affine surfaces for numerical models. One of typical self-affine surfaces (fractal dimension H=0.5) is shown in Figure 1 (a). Grid sizes on x-y plane varied from 64 to 256 to check the indenpendence of the analysis on grid size. Small scale roughness varied from 0 to 0.205 when grid size is defined by 1, and the radius R of the spherical surfaces varied from infinite (nominally flat) to 2.5L (L is the domain size).

3.2 Finite Element Analysis

We introduced finite element method (ABAQUS [13]) for the contact analysis. Typical finite element models have 70,000 nodes and 350,000 elements approximately.

Four-node tetrahedral elements were used. Due to the high computational cost, dynamic explicit method was used instead of standard implicit method. In the calculations, we considered the system size of L=128 mostly after the consistency check. Roughness Δ of 0.205 and radius R of 2.5L were also used in most simulations. Figure 1 (b) shows a typical finite element mesh for the simulations. Top body with curvature and roughness is deformable and bottom flat cube is perfectly rigid. We applied normal load at the top face of the deformable body, and dynamically relaxed the system to achieve equilibrium state.

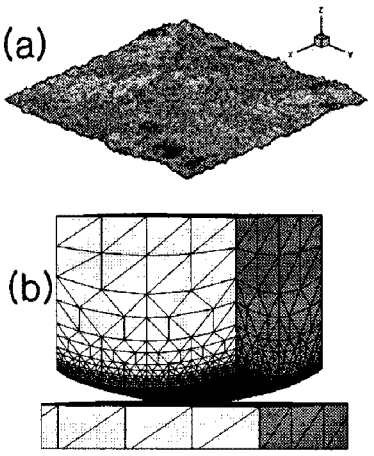

Figure 1: (a) Self-affine fractal surface image generated by the successive random midpoint algorithm. (b) Geometry of a finite element model in a deformable body (spherical top) with rough surface on a flat rigid substrate.

Contact conditions were fixed by hard contact (no penetration was allowed at the contact) without any interfacial interaction. To remove the boundary effects, we imposed periodic boundary conditions at the side faces. Two surfaces were considered in contact at each node if contact pressure was not zero. True contact area ratio ϕ was given by the ratio of the number of contact nodes over total number of nodes at the plane.

4. Results and discussions

4.1 Contact Properties for Spherical Surfaces

In Figure 2, typical contact patterns of spherical surfaces (R=2.5L) are shown for elastic and plastic

contacts when the contact area ratio ϕ is 0.1. Figure 2 (a) is for elastic contact with no roughness (Δ=0) and (b) is for elastic contact with roughness (Δ=0.205). For the rough contact (b), the pattern is complicated and many small contact clusters are widely spread, whereas the *smooth* contact (a) shows one circular area corresponds to ϕ=0.1.

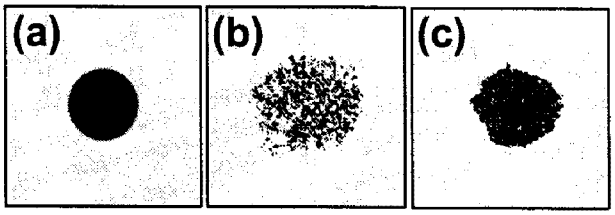

Figure 2: Actual patterns of contact area (=0.1) obtained from (a) elastic smooth sphere (b) elastic rough sphere, and (c) plastic (Cu) rough sphere. Note the apparent differences on the contact cluster shapes

On the other hand, Figure 2 (c) is for plastic contact with roughness (Δ =0.205). Its contact clusters are not widely distributed like (b), the contact pattern is still relatively complicated. We find the roughness generates wide distribution of normal load at the contact region, which may reduce the peak contact pressure.

4.2 External Load vs. True Contact Area

Figure 3 shows the relation between true contact area ratio (ϕ) vs. external normal load (P) for various roughness values Δ and radii R. In the plot, we added the analytic curve for smooth spherical contact [2] and for nominally flat contact with roughness [7] for comparisons.

From the power fitting with Eq. (3) on the numerical results, the exponents τ were obtained. The power exponent of elastic spherical surfaces is shown to vary from 0.67 to 0.90 as the roughness increases from 0 to 0.205. For fixed roughness Δ=0.205, the slope also shows strong dependence on the curvature. It is noted true contact area ratio depends on both geometrical parameters, the roughness and the nominal shape of contact surfaces.

In the same figure, we presented the result (open squares) for plastic contacts surfaces. When the plasticity is considered, the slope is nearly 20 times higher. And the fitted exponent τ is given by 0.83, which is apparently approaching to linear for the case of nominally flat surface [15]. Immediate plastic deformation at the contact region may reduce the curvature effect of the spherical contact surfaces.

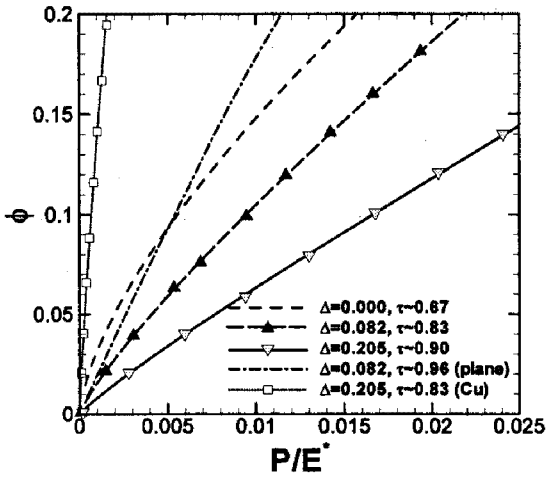

Figure 3: True contact area ratio ϕ vs. normalized external pressure P/E'. The fitted power exponent evolves from 0.67 (sphere) to 1.0 (nominally flat) as the roughness Δ increases.

4.3 Pressure Distributions of Elastic Contacts

Spatial distribution of local contact pressure provides key information to determine how the deformation may occur at the contact region by plastic deformation, fractures and failures. We investigated the pressure distribution as a function of true contact area and roughness, and presented in Figure 4 and Figure 5. Horizontal axis is for normalized radial distance (r/r_0) by effective radius $r_0(\equiv\sqrt{A/\pi})$ from the center of contact surface, and vertical axis is for normalized contact pressure (p/p_0) by external pressure p_0.

Figure 4 shows the contact pressure distribution as a function of roughness Δ. As the roughness increases from 0 to 0.205, the peak pressure inside the circular region drops from 1.5 to 0.5, and the pressure distribution however becomes gradually wider to reach outside the circular region (r/r_0>1). This behavior is consistent with the contact morphologies shown in Figure 2. It may imply the increase of roughness spreads the

external load efficiently over wide range of area, so that the peak contact pressure can be lowered.
In Figure 5, the contact pressure distribution of rough spheres (Δ=0.205) is shown as a function of contact area ratio, equivalent to external load). As the contact area ϕ varies from 0.05 to 0.3, the distribution curve approaches to the theoretical prediction for smooth spherical contact. By comparing it with Figure 4, the increase of contact area (or high external load) can induce similar effect on the distributions as the decrease of roughness. We suspect the separate contact clusters start to merge as the external load increases and the roughness effect becomes gradually negligible.

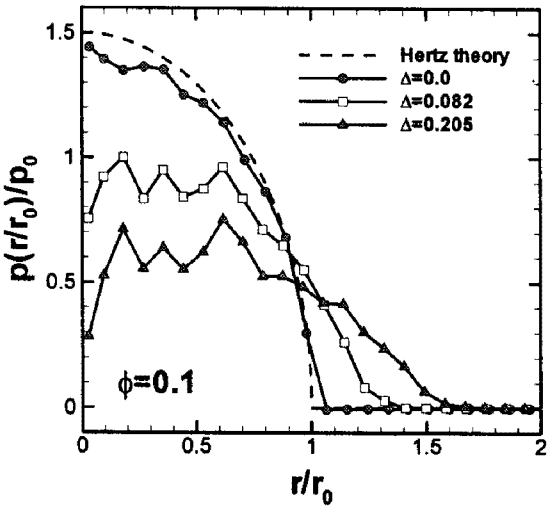

Figure 4: Radial distributions of contact pressure p. The distribution of contact pressure p is relatively wide at high roughness (Δ=0.205), while it is mostly confined in the limited region (r/r_0<1) at low roughness.

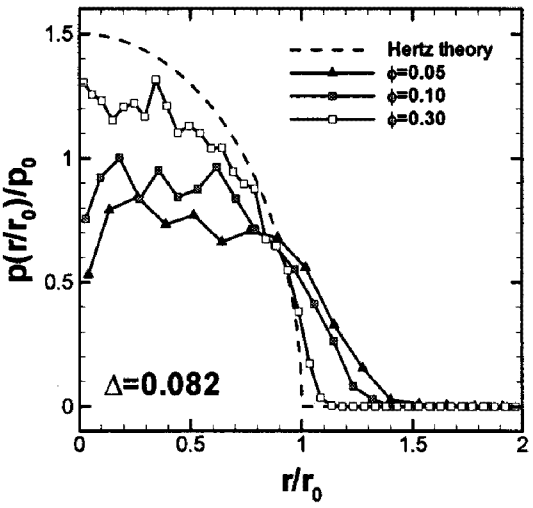

Figure 5: Radial distributions of contact pressure at different contact area. The pressure is more confined inside (r/r_0<1) as the true contact area increases.

4.4 Pressure Distributions of Plastic Contacts

Plasticity effect on the contact pressure distribution has been examined for the spherical rough contacts (Δ=0.205, R=2.5L). Material property of Cu was used in the finite element simulation, and the contact pressure distribution is shown in Figure 6.

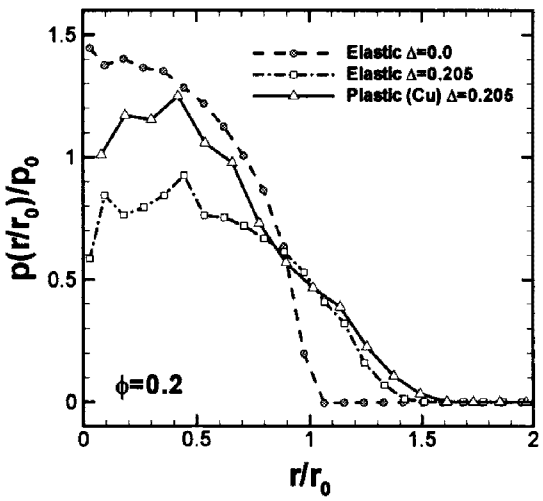

Figure 6: Radial distribution of pressure for real materials (Cu) with plasticity. It follows the distribution of rough surface outside (r/r_0>1) whereas it approaches to the smooth sphere inside

The distribution curve shows different behaviors at two separate regions. Outside of the circular region ($r/r_0>1$), it follows the elastic contact curve with same roughness. However, inside of the circular region ($r/r_0<1$), it is close to the elastic contact with no roughness ($\Delta=0$). It should be noticed, for the case of low yield stress (e.g., $Y_p/E' \sim 1/1100$ for Cu), plastic deformation at the contact asperities may reduce the roughness effect.

5. Conclusions

In this paper, we examined the dependence of contact properties on two geometrical parameters (curvature and roughness) of the spherical rough surfaces using numerical analysis. True contact area is obtained as power functions, and the fitted power exponent is sensitive to the parameters.

From the analysis on surface contact pressures, it is shown the peak contact pressure can drop by surface roughness. Wide distribution of the external pressure at the contact region may reduce the plastic failures when two surfaces are in mechanical contact.

In the present study, we neglected all interactions between contacting surfaces. However, for realistic simulations, interfacial forces such as adhesions, repulsions, and frictions should be considered especially in atomistic length scales [16]. In our finite element models, we could generate roughness at one surface only because normal load was considered. However, to address more practical contact phenomena such as frictions, it is required to apply shear loads on two rough surfaces. We are currently working on the development of more general simulation frameworks.

Acknowledgments

This work was supported by the Grant of the Korean Ministry of Education, Science and Technology (The Regional Core Research Program/Medical Convergence Technology Development Consortium for Anti-aging and Well-being). One of the authors (S.H.) thanks M. O. Robbins for the support of visiting program at Johns Hopkins University.

References

[1] F. P. Bowden and D. Tabor, 1986, *The Friction and Lubrication of Solids*, Oxford, Clarendon Press.

[2] J. A. Greenwood, 1984, *Proc. R. Soc. London, Ser. A* Vol. 393, p.133.

[3] B. N. J. Persson, 2001, *Phys. Rev. Lett.* Vol. 87, p.116101.

[4] K. L. Johnson, 1985, *Contact Mechanics*, New York, Cambridge University Press.

[5] J. A. Greenwood and J. B. P. Williamson, 1966, *Proc. R. Soc. London, Ser. A* Vol. 295, p.300.

[6] A. W. Bush, R. D. Gibson, and T. R. Thomas, 1975, *Wear* Vol. 35, p.87.

[7] S. Hyun, L. Pei, J. F. Molinari, and M. O. Robbins, 2004, *Phys. Rev. E* Vol. 70, p.26117.

[8] J. H. Dieterich and B. D. Kilgore, 1994, *Pure Appl. Geophys.* Vol. 143, p.283.

[9] J. Krim and G. Palasantzas, 1995, *Int. J. Mod. Phys. B* Vol. 9, p.599.

[10] P. Berthoud and T. Baumberger, 1998, *Proc. R. Soc. London, Ser. A* Vol. 454, p.1615.

[11] B. B. Mandelbrot, 1979, *The Fractal Geometry of Nature*, New York, Freeman.

[12] R. F. Voss, 1985, *Random fractal forgeries*, Berlin, Springer-Verlag, p. 805.

[13] ABAQUS, product of HKS, Inc..

[14] T. Belytschko and T. J. R. Hughes, 1983, *Computational Methods for Transient Analysis*, Amsterdam, North-Holland.

[15] L. Pei, S. Hyun, J. F. Molinari, and M. O. Robbins, 2004, J. Mech. Phys. Solids (in press).

[16] Binquan Luan and M. O. Robbins, 2005, Nature, Vol.435, p.929.